Monthly Notices
of the
ROYAL ASTRONOMICAL SOCIETY

MNRAS **471,** 2703–2714 (2017) doi:10.1093/mnras/stx1730
Advance Access publication 2017 July 15

Single-dish and VLBI observations of Cygnus X-3 during the 2016 giant flare episode

E. Egron,[1⋆] A. Pellizzoni,[1] M. Giroletti,[2] S. Righini,[2] M. Stagni,[2] A. Orlati,[2] C. Migoni,[1] A. Melis,[1] R. Concu,[1] L. Barbas,[3] S. Buttaccio,[4] P. Cassaro,[4] P. De Vicente,[3] M. P. Gawroński,[5] M. Lindqvist,[6] G. Maccaferri,[2] C. Stanghellini,[2] P. Wolak,[5] J. Yang,[6] A. Navarrini,[1] S. Loru,[1] M. Pilia,[1] M. Bachetti,[1] M. N. Iacolina,[1,7] M. Buttu,[1] S. Corbel,[8,9] J. Rodriguez,[8] S. Markoff,[10] J. Wilms,[11] K. Pottschmidt,[12,13] M. Cadolle Bel,[14] E. Kalemci,[15] T. Belloni,[16] V. Grinberg,[17] M. Marongiu,[1,18] G. P. Vargiu[1] and A. Trois[1]

[1]*INAF, Osservatorio Astronomico di Cagliari, Via della Scienza 5, I-09047 Selargius, Italy*
[2]*INAF, Istituto di Radio Astronomia di Bologna, Via P. Gobetti 101, I-40129 Bologna, Italy*
[3]*Centro Nacional de Tecnologías Radioastronómicas y Aplicaciones Geoespaciales (CNTRAG), Observatorio de Yebes (IGN), Apartado 148, E-19080, Yebes (Guadalajara), Spain*
[4]*INAF, Istituto di Radioastronomia, Sezione di Noto, Contrada Renna Bassa, I-96017 Noto, Italy*
[5]*Centre for Astronomy, Faculty of Physics, Astronomy and Informatics, Nicolaus Copernicus University, Grudziadzka 5, PL-87-100 Torun, Poland*
[6]*Department of Earth and Space Sciences, Onsala Space Observatory, Chalmers University of Technology, SE-439 92 Onsala, Sweden*
[7]*Agenzia Spaziale Italiana – Via del Politecnico snc, I-00133 Roma, Italy*
[8]*Laboratoire AIM, UMR 7158, CEA/CNRS/Université Paris Diderot, CEA DRF/IRFU/DAp, F-91191 Gif-sur-Yvette, France*
[9]*Station de Radioastronomie de Nançay, Observatoire de Paris, PSL Research University, CNRS, Univ. Orléans, F-18330 Nançay, France*
[10]*Anton Pannekoek Institute for Astronomy, University of Amsterdam, PO Box 94249, NL-1090 GE Amsterdam, the Netherlands*
[11]*Dr. Karl-Remeis-Sternwarte and Erlangen Centre for Astroparticle Physics (ECAP), Friedrich Alexander Universität Erlangen-Nürnberg, Sternwartstr 7, D-96049 Bamberg, Germany*
[12]*CRESST and NASA Goddard Space Flight Center, Astrophysics Science Division, Code 661, Greenbelt, MD 20771, USA*
[13]*Center for Space Science and Technology, University of Maryland Baltimore County, 1000 Hilltop Circle, Baltimore, MD 21250, USA*
[14]*Max Planck Computing and Data Facility, D-85748 Garching, Germany*
[15]*Faculty of Engineering and Natural Sciences, Sabancı University, Orhanlı-Tuzla, 34956 Istanbul, Turkey*
[16]*INAF, Osservatorio Astronomico di Brera, via E. Bianchi 46, I-23807 Merate, Italy*
[17]*ESA/ESTEC, Keplerlaan 1, NL-2201 AZ Noordwijk, The Netherlands*
[18]*Department of Physics and Earth Sciences, University of Ferrara, via Saragat 1, I-44122 Ferrara, Italy*

Accepted 2017 July 7. Received 2017 June 21; in original form 2017 May 2

ABSTRACT

In 2016 September, the microquasar Cygnus X-3 underwent a giant radio flare, which was monitored for 6 d with the Medicina Radio Astronomical Station and the Sardinia Radio Telescope. Long observations were performed in order to follow the evolution of the flare on an hourly scale, covering six frequency ranges from 1.5 to 25.6 GHz. The radio emission reached a maximum of 13.2 ± 0.7 Jy at 7.2 GHz and 10 ± 1 Jy at 18.6 GHz. Rapid flux variations were observed at high radio frequencies at the peak of the flare, together with rapid evolution of the spectral index: α steepened from 0.3 to 0.6 (with $S_\nu \propto \nu^{-\alpha}$) within 5 h. This is the first time that such fast variations are observed, giving support to the evolution from optically thick to optically thin plasmons in expansion moving outward from the core. Based on the Italian network (Noto, Medicina and SRT) and extended to the European antennas (Torun, Yebes, Onsala), very long baseline interferometry (VLBI) observations were triggered at 22 GHz on five different occasions, four times prior to the giant flare, and once during its decay phase. Flux variations of 2 h duration were recorded during the first session. They correspond to a mini-flare that occurred close to the core 10 d before the onset of the giant flare. From the latest VLBI observation we infer that 4 d after the flare peak the jet emission was extended over 30 mas.

Key words: stars: flare – stars: individual: Cyg X-3 – radio continuum: stars – X-rays: binaries.

⋆ E-mail: egron@oa-cagliari.inaf.it

1 INTRODUCTION

Galactic X-ray binaries with jets are called microquasars, in analogy to the phenomena seen in quasars but on much smaller scales (Mirabel & Rodríguez 1999). Most microquasars host a stellar-mass black hole as the compact object. They spend most of their time in a dormant state and suddenly enter into periods of outburst activity. Major progress has been made in the understanding of the accretion/ejection connections thanks to multiwavelength observations. However, the formation of relativistic jets, their composition and exact launching mechanisms are still poorly known.

Discovered by Giacconi et al. (1967) at the dawn of X-ray astronomy, Cygnus X-3 (Cyg X-3) is a rare high-mass X-ray binary consisting of a compact object wind-fed by a Wolf–Rayet star (van Kerkwijk et al. 1996; Fender, Hanson & Pooley 1999; Koch-Miramond et al. 2002). The nature of the compact object is still uncertain, but a black hole seems to be favoured considering X-ray and radio emissions (Hjalmarsdotter et al. 2009; Shrader, Titarchuk & Shaposhnikov 2010, and references therein). Located in the Galactic plane at a distance of 7–9 kpc (Predehl et al. 2000; Ling, Zhang & Tang 2009; McCollough, Corrales & Dunham 2016), Cyg X-3 has a short orbital period of 4.8 h (Parsignault et al. 1972). It is a reasonably strong persistent radio source with a typical flux of about 100–200 mJy in the quiescent state (Waltman et al. 1996). Flares of various amplitudes are frequently detected, classified as minor or major flares according to the flux density below or above 1 Jy. Quenched radio states (<30 mJy; Waltman et al. 1996) are occasionally observed for Cyg X-3. They are usually followed by major radio flares on a scale of a few days or weeks (Waltman et al. 1994, 1995). Radio fluxes of 10–20 Jy associated with giant flare events have been measured, with an increasing flux of a factor ∼1000 in a few days (Waltman et al. 1995; Mioduszewski et al. 2001; Miller-Jones et al. 2004; Corbel et al. 2012). No other X-ray binary has shown such strong and uncommon flux densities up to 20 Jy, which makes Cyg X-3 the brightest X-ray binary at radio frequencies. One- and two-sided relativistic jets with a complex structure were clearly resolved during these episodes using the Very Long Array (VLA), the Very Long Baseline Array (VLBA) and the European Very Long Baseline Interferometry Network (e-EVN) (Martí, Paredes & Peracaula 2001; Mioduszewski et al. 2001; Miller-Jones et al. 2004; Tudose et al. 2007).

X-ray data from Cyg X-3 is more complex compared to other X-ray binaries (Bonnet-Bidaud & Chardin 1988; Szostek & Zdziarski 2008; Koljonen et al. 2010). Strong X-ray absorption at low energies is likely associated with the dense wind of the companion star (Szostek & Zdziarski 2008). Despite the complex spectral behaviour, observations have demonstrated that the source exhibits the canonical X-ray states (hard, intermediate and soft states; McClintock & Remillard 2006; Belloni 2010) in addition to the very high state and the ultra-soft state (Szostek & Zdziarski 2004; Hjalmarsdotter et al. 2009). The connections between the X-ray (accretion) and radio (ejections) emission of Cyg X-3 have been widely studied (Watanabe et al. 1994; McCollough et al. 1999; Gallo, Fender & Pooley 2003; Hjalmarsdotter et al. 2008; Szostek, Zdziarski & McCollough 2008; Zdziarski, Segreto & Pooley 2016). In particular, giant radio flares correspond to the transition from the ultra-soft state to a harder X-ray state (Koljonen et al. 2010).

Cyg X-3 was also the first microquasar detected in gamma-rays with AGILE and *Fermi*/LAT (Fermi LAT Collaboration 2009; Tavani et al. 2009), providing unique insight into the particle acceleration up to GeV energies during the ejection. Gamma-ray emission was detected by *Fermi*/LAT during the 2011 giant flare episode (Corbel et al. 2012). The high-energy emission (>100 MeV) corresponds to transitions in and out of ultra-soft X-ray state.

The Sardinia Radio Telescope (SRT[1]) has carried out a large-monitoring program of several X-ray binaries during the Early Science Program (ESP[2]), from 2016 February to July (PI: Egron). The weekly monitoring performed at 7.2 and 22 GHz has shown that Cyg X-3 was in the quiescent state during this period. A quenched radio state was detected by the RATAN-600 on 2016 August 23–25 (Trushkin et al. 2016a), five and a half years after its last quenched episode. The ultra-soft X-ray state was confirmed by *Swift*/BAT,[3] which registered a strong decrease of a factor 25 of the hard X-ray emission in the 15–50 keV band in less than 10 d, from August 15 to August 24. The AGILE-GRID detector revealed gamma-ray emission above 100 MeV consistent with the position of Cyg X-3 on August 28–30 (Piano et al. 2016). The strong increase of the radio flux occurred from September 14, 3 weeks after the transition to the quenched radio state (Trushkin et al. 2016a,b). A gamma-ray flare was detected by *Fermi*/LAT the same days, on September 15–16 (Cheung & Loh 2016).

In this paper, we present single-dish and very long baseline interferometry (VLBI) observations of Cyg X-3 corresponding to the 2016 September giant flare episode. We present the details of the observations and data reduction in Section 2, the evolution of the flux density and spectral index in Section 3, and discuss the results we obtained, in particular the jet characteristics and morphologies associated with the mini and giant flares in Section 4.

2 OBSERVATIONS AND DATA REDUCTION

We initially planned to perform VLBI observations to catch the source during the rising and declining phases of the flare in order to track the evolution of the relativistic jets. Due to the difficulty to trigger VLBI observations in a very short time (considering the availability of the antennas), we conducted single-dish observations at the moment of the peak of the flare (Egron et al. 2016a). The recently commissioned 64 m-SRT (Bolli et al. 2015; Prandoni et al. 2017) participated in both single-dish and VLBI observations, together with the 32 m-Medicina radio telescope. VLBI observations included SRT, Medicina, Noto, Torun, Yebes and Onsala in order to provide a larger coverage of the (u, v)-plane.

2.1 Single-dish observations

A Target-of-Opportunity program for Cyg X-3 was triggered by the Italian Medicina Radio Astronomical Station and SRT single dishes. The outburst was followed from 2016 September 17 to 2016 September 23. Both antennas were equipped with the same control software designed to optimize single-dish observations (Orlati et al. 2016). The frequency agility (switching the observing frequencies in only a few minutes) coupled with the different SRT and Medicina receivers enabled a large frequency coverage of Cyg X-3 during the flare, from 1.5 to 25.6 GHz.

SRT observations were carried out at 1.5 GHz (L band), 7.2 GHz (C band) and 22.7 GHz (K band) using the Total Power and SARDARA (Melis et al. in preparation) backends in piggy-back mode. Observations consist of rectangular and perpendicular On-The-Fly

[1] www.srt.inaf.it
[2] www.srt.inaf.it/astronomers/early-science-program-FEB-2016/
[3] See Krimm et al. (2013) for a description of the *Swift*/BAT transient monitor.

Table 1. Beam sizes at the observed frequencies using SRT and Medicina as single-dish radio telescopes.

Radio telescope	Frequency (GHz)	Beam size (arcmin)
SRT	1.5	12.2
	7.2	2.63
	22.7	0.816
Medicina	8.5	4.55
	18.6	2.08
	25.6	1.51

(OTF) maps performed in the right ascension (RA) and declination (Dec.) directions (forming a Greek cross map), at constant velocity (4 arcmin s^{-1}). The dimensions of the maps were chosen according to the beam size (see Table 1) at the observed frequencies: $1.^{\circ}5 \times 0.^{\circ}6$ at 1.55 GHz, $0.^{\circ}5 \times 0.^{\circ}12$ at 7.2 GHz and $0.^{\circ}2 \times 0.^{\circ}05$ at 22.7 GHz. This method has been applied during the Early Science Program dedicated to the monitoring of X-ray binary systems. The observing strategy has the advantage of providing a direct image of the sources in the vicinity of the target and a better estimate of the flux density. The data analysis was accomplished with the SRT Single-Dish-Imager (Egron et al. 2016b), a software designed to perform automated baseline subtraction, radio interference rejection and calibration. The spectral flux density of the target was reconstructed by observing three calibrators (3C286, 3C295 and 3C48) at all frequencies, by applying the values and polynomial expressions proposed by Perley & Butler (2013).

Cyg X-3 was observed with Medicina at 8.5 GHz (*X* band), 18.6 GHz and 25.6 GHz (*K* band), using the OTF cross-scan technique in RA and Dec. directions. In *X* band, the bandwidth was 680 MHz with a scan length and velocity of $0.^{\circ}6$ and 2.4 arcmin s^{-1}, respectively, while in *K* band we selected a bandwidth of 1200 MHz, scans of $0.^{\circ}2$ length and a scan velocity of 0.8 arcmin s^{-1}. We applied gain curve and pointing offset corrections to the measurements. Additional opacity and atmospheric corrections were added in the case of *K*-band data (18.6 and 25.6 GHz). The flux calibration was performed with observations of 3C286, 3C48 and NGC7027. The flux of 3C286 was calculated according to Perley & Butler (2013), while the fluxes of the other calibrators were reckoned on the basis of Ott et al. (1994). The single-dish observations are reported in Table 2.

2.2 VLBI observations

We triggered five VLBI observations on Cyg X-3, from the quenched radio state until the end of the strong flare episode. Our aim was to catch the target in the rising and fading phases of the predicted giant flare (Trushkin et al. 2016a) in order to follow the evolution of the relativistic jets. The first two VLBI observations were triggered on 2016 September 1 and 3, right after the first increase of the hard X-ray emission recorded by the *Swift*/BAT on 2016 August 29. It turned out that the X-ray flux decreased 3 d later and the giant flare did not occur at that time. We triggered other VLBI observations a few days later, on 2016 September 9 and 10, after a second increase of the X-ray flux on September 8. The last observation was carried out on September 23, during the declining phase of the giant radio flaring episode. The observing sessions are indicated in the bottom panel of the Fig. 1.

The VLBI observations were performed at 22 GHz with the following radio telescopes, according to their availability: SRT (Sr), Medicina (Mc), Noto (Nt, 32 m, Italy), Torun (Tr, 32 m, Poland),

Table 2. Single-dish observations of Cyg X-3 performed with Medicina at 8.5, 18.6 and 25.6 GHz, and with SRT at 1.5, 7.2 and 22.7 GHz.

Obs. date	MJD	Frequency (GHz)	Flux density (Jy)
2016 September 17	57648.86	8.5	13.1 ± 0.4
	57648.88		12.9 ± 0.4
	57648.90		13.0 ± 0.4
	57648.92		12.9 ± 0.4
	57648.95	18.6	7.5 ± 0.8
	57648.97	25.6	7.0 ± 0.7
2016 September 19	57650.62	7.2	12.0 ± 0.6
	57650.65	8.5	12.9 ± 0.4
	57650.67		12.9 ± 0.4
	57650.67	7.2	12.6 ± 0.6
	57650.70		13.1 ± 0.7
	57650.70	18.6	8.9 ± 0.9
	57650.71	7.2	12.8 ± 0.6
	57650.72	22.7	9.5 ± 0.9
	57650.73	18.6	10 ± 1
	57650.77	7.2	13.2 ± 0.7
	57650.88		12.8 ± 0.6
	57650.91		12.9 ± 0.6
	57650.91	25.6	6.1 ± 0.6
	57650.93		5.6 ± 0.6
	57650.95	22.7	6.4 ± 0.6
2016 September 20	57651.54	7.2	11.4 ± 0.6
	57651.61	8.5	12.1 ± 0.4
	57651.63	7.2	11.8 ± 0.6
	57651.65	18.6	7.2 ± 0.7
	57651.68	25.6	7.3 ± 0.7
2016 September 21	57652.67	7.2	6.9 ± 0.3
	57652.72	22.7	3.6 ± 0.4
	57652.76	1.5	14.4 ± 0.5
2016 September 22	57653.97	8.5	3.2 ± 0.1
	57653.99		3.1 ± 0.1
2016 September 23	57654.00	8.5	3.1 ± 0.1

Yebes (Ys, 40 m, Spain) and Onsala (On, 20 m, Sweden). We alternately observed Cyg X-3 and the calibrators 3C345, BL Lac, J2007+4029 and J2015+3710, resulting in sessions of 7–15.5 h each. The data were processed with the DiFX correlator (Deller et al. 2011) installed and operated in Bologna. The VLBI analysis was performed with the Astronomical Image Processing System (Greisen 2003). The calibrator J2007+4029 was used to perform the phase referencing. The phase-referencing cycle was 4 min:2.5 min on the target and 1.5 min on phase-cal. Since the calibrator-target separation was quite large ($d = 4.^{\circ}7$), and the region is subject to significant scatter, we also observed the check source J2015+3710 every 30 min. This source was also phase-referenced to J2007+4029 and it was used to confirm that the phase solutions were transferred correctly. We also tried to fringe-fit the Cyg X-3 data directly, in order to estimate its signal-to-noise ratio in each 2.5 min long scan. However, these results were rather used for data quality assessment than for further analysis.

3 RESULTS

3.1 Single-dish monitoring of the giant flare

Medicina and SRT provided the monitoring of Cyg X-3 from September 17 to September 23 at 1.5, 7.2, 8.5, 18.6, 22.7 and 25.6 GHz, which was complementary to the daily monitoring of the source performed with the RATAN-600 (covering the 2.3, 4.6, 8.2,

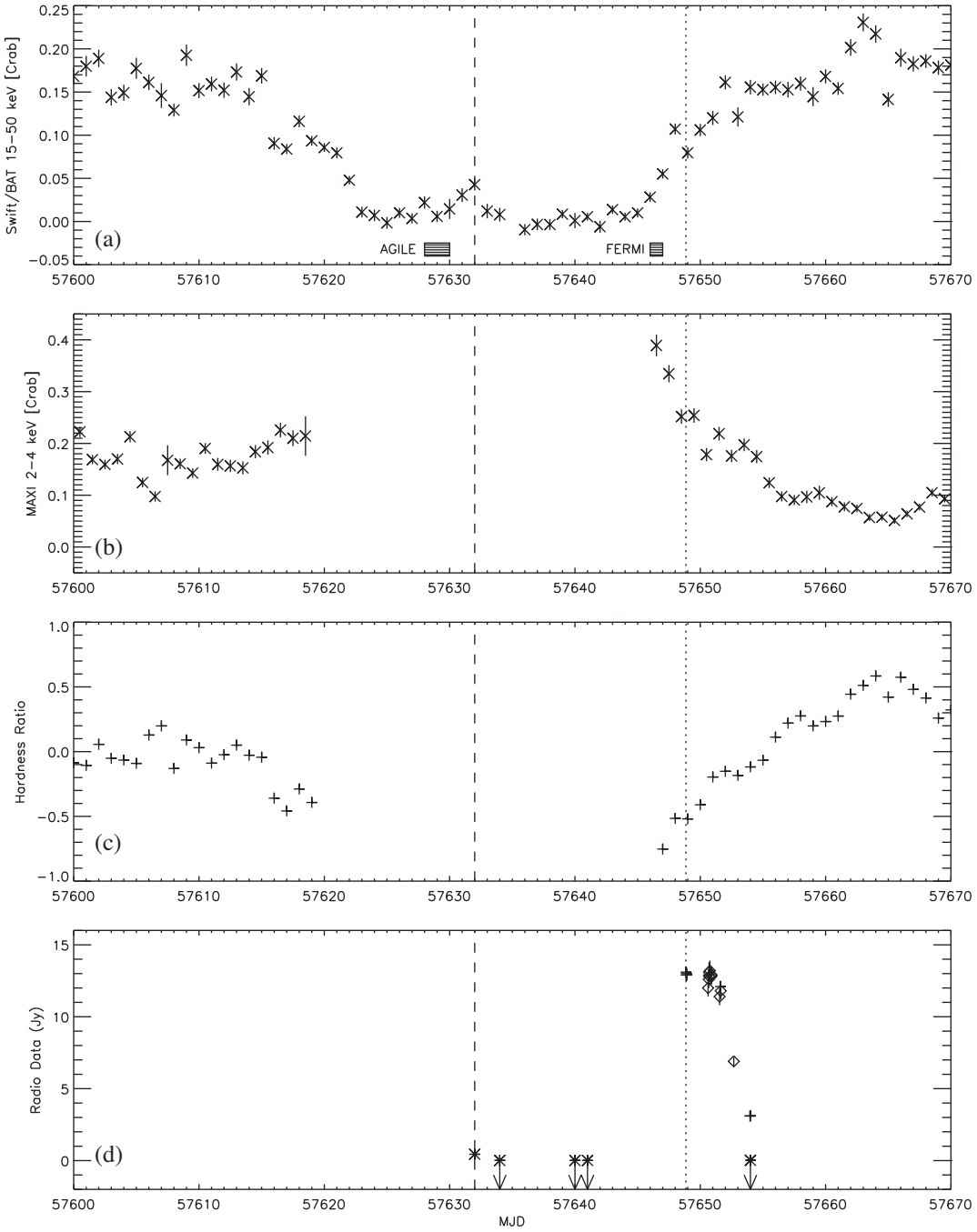

Figure 1. From the top to the bottom: (a) *Swift*/BAT 15–50 keV (Hard X-rays) light curve of Cyg X-3 in Crab units from 2016 July 31 to 2016 October 9. The gamma-ray detections with AGILE and *Fermi*/LAT are also reported; (b) MAXI 2–4 keV (Soft X-rays) light curve in Crab units; (c) hardness ratio corresponding to (Hard−Soft)/(Hard+Soft); (d) single-dish (cross: 8.5 GHz; diamond: 7.2 GHz) and VLBI data at 22 GHz (asterisk). The dashed line and the dotted line indicate the first VLBI observation and the first single-dish observation, respectively. The vertical arrows represent the VLBI upper limits at 5σ confidence.

11.2, 21.7 GHz frequencies; Trushkin et al. 2017). Our observations are summarized in Table 2 and represented in Fig. 1, together with the X-ray light curves obtained with data daily averages from *Swift*/BAT at 15–50 keV and MAXI at 2–4 keV in Crab units.[4] The hardness ratio obtained from *Swift*/BAT and MAXI data is also reported despite the lack of MAXI data during most of the ultra-soft X-ray state, even though present in the *Swift*/BAT light curve.

The giant radio flare reached its highest brightness on 2016 September 19 (MJD 57650.7). While the flux density remained quite stable (∼13 Jy) at 7.2–8.5 GHz during the peak maximum, we observed flux variations on the time-scale of a few hours in *K* band, as shown in Figs 2 and 3 (note that all error bars are at the 1σ level). The 18.6, 22.7 and 25.6 GHz observations performed independently (observational and data reduction techniques) with

[4] 1 Crab = 0.22 ct cm^{-2} s^{-1} for the *Swift*/BAT rate and 1 Crab = 1.67 ct cm^{-2} s^{-1} for the MAXI rate.

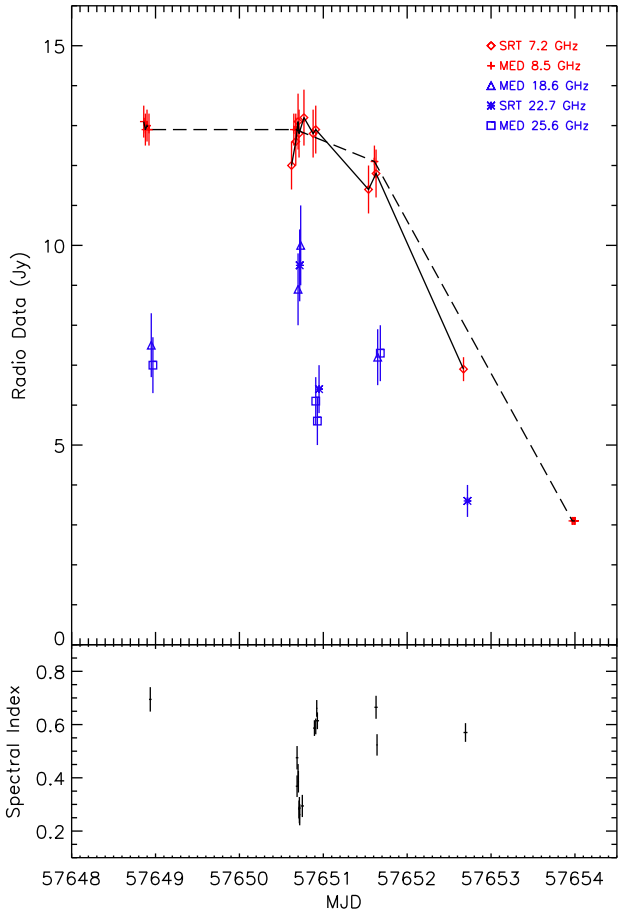

Figure 2. Top panel: Medicina and SRT observations covering the peak of the giant flare (see Table 2 for more details). Lower frequencies are indicated in red while higher frequencies are in blue. Bottom panel: Evolution of the spectral index α.

Medicina and SRT are perfectly consistent, demonstrating a decrease of the flux within less than 5 h before it increased again the day after, on September 20. On the other hand, the radio emission at 7.2–8.5 GHz severely weakened from September 20; a reduction of ∼9 Jy is detected within 2.4 d. Observations carried out with the SRT on September 21 at 1.5, 7.2 and 22.7 GHz indicated that the ejection is optically thin, as shown in Fig. 4.

The evolution of the spectral index α (with $S_\nu \propto \nu^{-\alpha}$) is shown in Fig. 2. The spectral indexes were calculated by considering all couples of flux density measurements available at low and high frequencies (7.2–8.5 and 18.6–25.6 GHz) within 1 h from each other. Spectral index errors were derived from error propagation of flux density errors for each couple. The time tag of the reported spectral index values corresponds to the mid-time between the epochs of each flux density measurement couple. The error bars on the x-axis (time) reflects the epoch separation for each couple of flux density measurements. We clearly observed a spectral steepening from $\alpha = 0.34 \pm 0.08$ to 0.61 ± 0.03 within ∼5 h at the moment of the peak maximum of the flare. In Fig. 3, we show a zoom of the light curve and spectral index evolution for the observation of 2016 September 19 (MJD 57650).

3.2 VLBI results

Compact (milliarcsecond scale) radio emission was detected from Cyg X-3 during the first VLBI observation, on 2016 September 1.

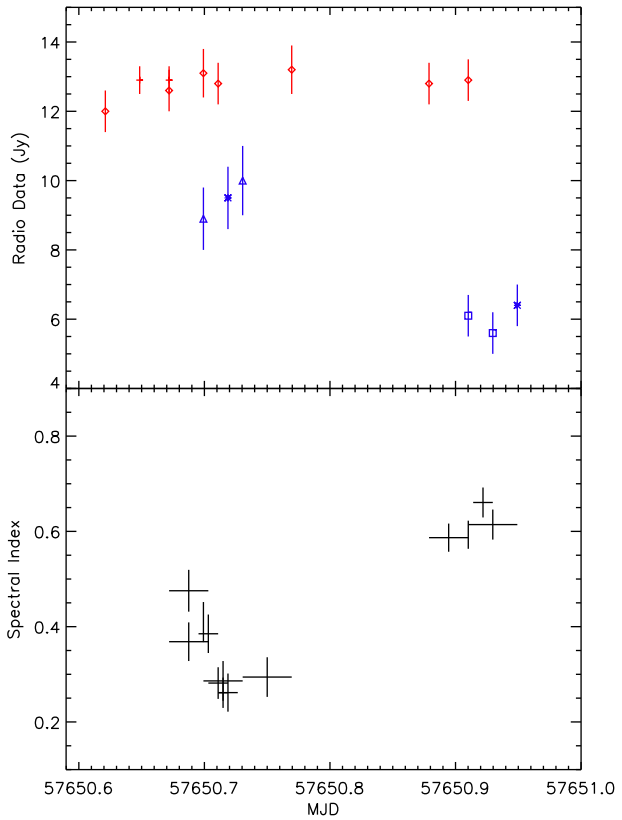

Figure 3. Zoom of the light curve and spectral index evolution presented in Fig. 2 during the maximum of the giant flare peak, on 2016 September 19.

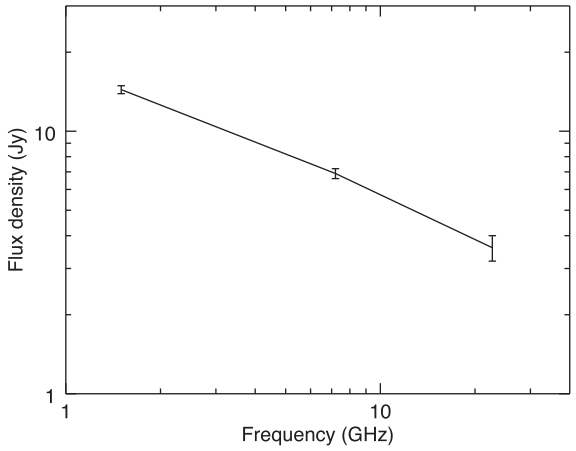

Figure 4. Optically thin spectrum obtained from SRT data at 1.5, 7.2 and 22.7 GHz 2 d after the maximum of the giant flare.

This detection was confirmed both for the phase-referenced visibilities, whose amplitude and phase showed well-defined coherence, and from a run of fringe fitting directly to the source itself, which produced good solutions for all the intervals with valid data.

In Fig. 5, we show visibility amplitude and phase versus time for all the baselines to SRT. Other baselines show similar behaviour but with increased scatter due to lower baseline sensitivity. We note a variable total flux density: the amplitudes are in general higher in the first half of the session than in the second. Moreover, there is clear variability on hour-scale in the initial 4 h of the observation. We exclude the possibility that this variability is instrumental: we

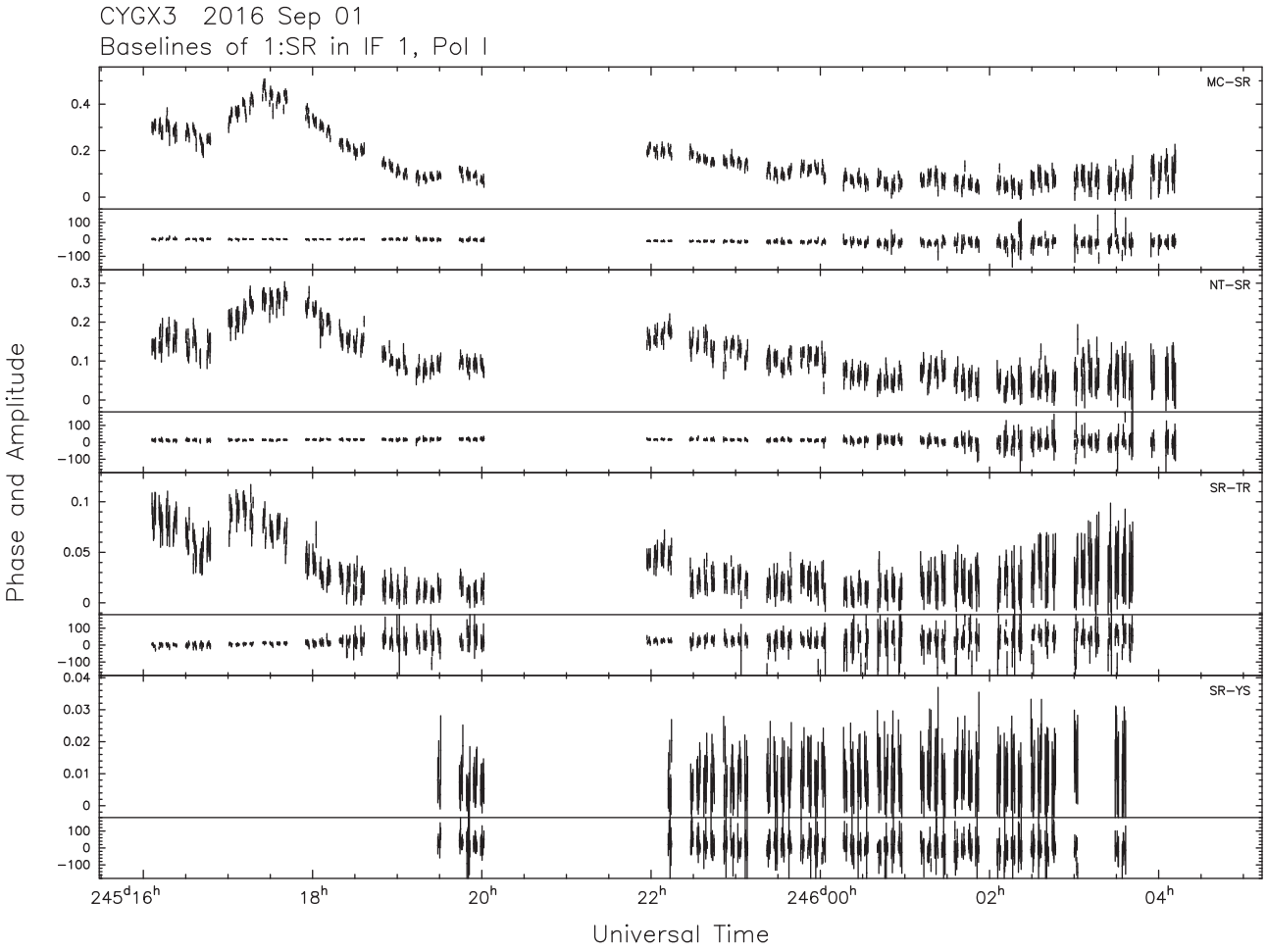

Figure 5. Cyg X-3 visibility amplitude and phase versus time for baselines to SRT for the 2016 September 1 (MJD 57632) observations at 22 GHz. Four pairs of panels are shown; from top to bottom: Sr-Mc, Sr-Nt, Sr-Tr, Sr-Ys; in each pair, the top panel shows amplitudes (in Jy) and the bottom phases (in degrees). Data are missing at around UT 21 for these baselines, due to SRT elevation limits (source transiting at zenith), but are in general present on other baselines. Note that the first part of the observation was missed by Yebes due to technical problems.

present in Fig. 6 the visibility amplitudes (Mc-Sr, Nt-Sr, Sr-Tr baselines) for Cyg X-3 and J2007+4920 for the first 4 h of observations. The comparison source shows the stability of the system, which allows us to infer that the amplitude variation is intrinsic to Cyg X-3. Moreover, the variations follow the same pattern on baselines of very different orientations in the (u, v)-plane (including those not shown: Mc-Nt, Mc-Tr, Nt-Tr). This behaviour indicates that the amplitude variability is not due to the source structure but rather to intrinsic flux density variations.

The short-scale time variability prevents us from obtaining a meaningful average image for the whole observation, as the imaging algorithms in interferometry produce a Fourier transform of the visibility amplitude and phase in the (u, v)-plane to the brightness in the sky combining all visibilities together. Different portions of the (u, v)-plane are therefore sampled at different times. When the source varies during the duration of the observation, the transform of the (u, v)-plane consequently becomes ill-posed. For this reason, it is not possible to produce a meaningful image of the source from the entire data set during our VLBI observation. A possibility would be to produce images for short time intervals, during which we can assume that variability plays a negligible role. However, in this case we can only use the visibilities acquired during that time interval, which means that we only sample a small portion of the (u, v)-plane. As a result, the image quality becomes very poor (in particular for our sparse array of only four to five stations). This is the reason why we resorted to model-fitting in the (u, v)-plane rather than to images. We model-fit the visibility within each time bin of 15 min by using a circular Gaussian model of 1.5 mas Half Power Beam Width (HPBW) (the beam would naturally be elliptical; note that the real beam size during this observation was 1.50 mas × 0.97 mas) in which we let position, amplitude and width free to vary. It is therefore possible to study the evolution of the size of the emitting component, at least during the first 4 h of the observation when we had a better signal-to-noise ratio to constrain the fit. The size of the emitting region increased with time from 0.6 to 0.9 mas radius, as shown in Figs 7 and 8. After 20.00 UT on 2016 September 1, the size becomes smaller. This shrinking is most likely an artefact due to the low signal-to-noise ratio. Another intriguing possibility is that the beam position angle is rotating from a direction aligned with the jet axis to a transverse one, so we see a narrower size.

We have created both clean images and visibility data models for each time bin of 15 min and determined the target's flux density using both methods. The resulting overall trends are entirely consistent. We report in Fig. 9 the numbers provided by visibility model fits. Two small peaks of ∼440 and ∼250 mJy flux density are clearly visible in the light curve, both with a 2 h duration. We

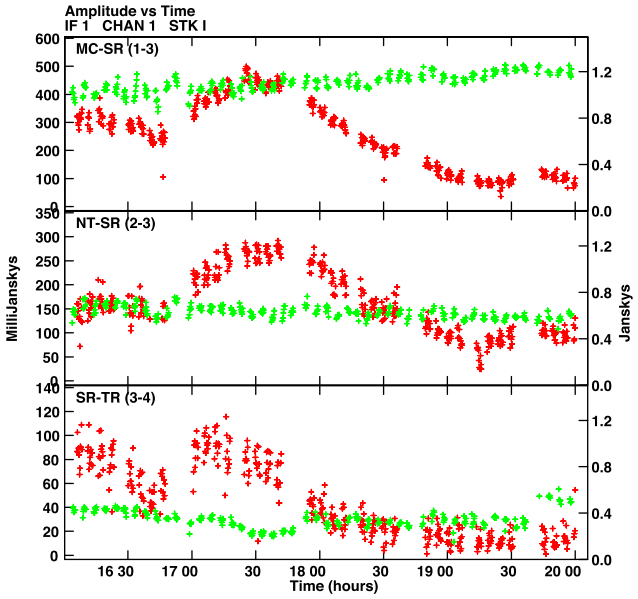

Figure 6. Visibility amplitudes of Cyg X-3 (red) and J2007+4029 (green) during the four first hours of the 2016 September 1 observation (MJD 57632). Variability is observed on the Mc-Sr, Nt-Sr, Sr-Tr baselines for Cyg X-3 within 2 h whereas the comparison source remains stable.

catched a mini-flare of Cyg X-3 instead of the expected giant flare event. The flux density variability on sub-hour scales is however clearly present and it is intrinsic to the source, as demonstrated in Fig. 6.

The following VLBI observations triggered on 2016 September 3, 9 and 10 did not provide any detection of Cyg X-3 (upper limit of 8 mJy at 5σ), as confirmed by the analysis in both the visibility and the image domains. In the visibility domain, after transferring phase solutions from the calibrator, we tried to fringe fit the source visibilities, finding no solution. After directly imaging the

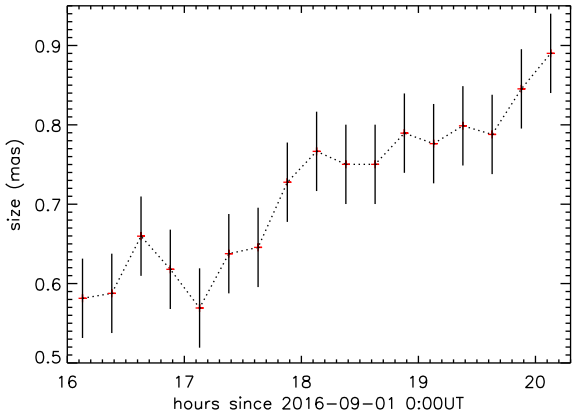

Figure 8. Radius in mas of the emitting component versus time corresponding to Fig. 7. The size increased within 4 h, which indicates a signature of the expansion of the emitting region.

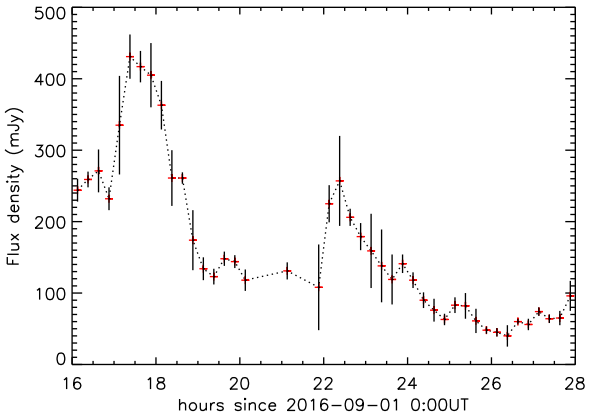

Figure 9. VLBI light curve obtained on 2016 September 1 (MJD 57632) showing a short-scale time variability, with the evidence of two peaks of different flux density during a mini-flare. The general trend of the off-peak measurements indicates a decrease of the flux during the observation.

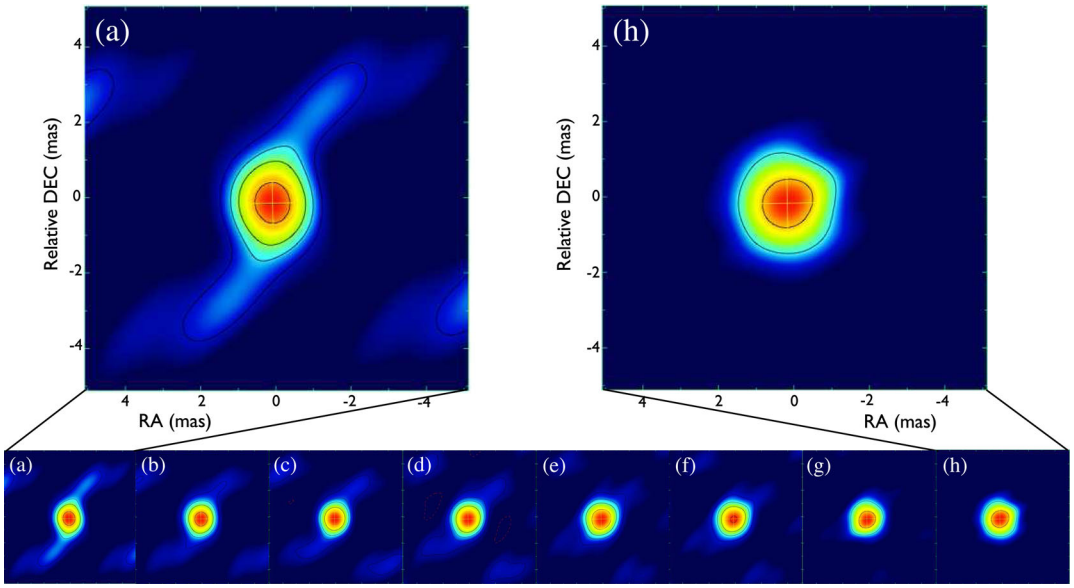

Figure 7. Evolution of the size of the emitting component during the first 4 h of the VLBI observation performed on 2016 September 1 (MJD 57632). The images were obtained on short time intervals of 15 min by convolving the best-fitting circular Gaussian with a circular beam of 1.5 mas HPBW. A sequence of images from (a) to (h) is represented, with an interval of 30 min between two consecutive images for clarity. The first (a) and last (h) images correspond to 16:15 UT and 20:00 UT, respectively.

Table 3. VLBI observations of Cyg X-3 performed at 22 GHz with SRT, Medicina, Noto, Torun, Yebes and Onsala. MJD start and end indicate the beginning and the end of each session while the effective time is related to the observation time on Cyg X-3. Upper limits are given at 5σ when the source was not detected at the known position.

Radio telescopes	Obs. date	MJD (start)	MJD (end)	Flux density (mJy)
Sr, Mc, Nt, Tr, Ys	2016 September 1	57632.67	57632.79[a]	440
		57632.79[a]	57633.21	250
Sr, Mc, Nt, Tr, Ys	2016 September 3	57634.67	57635.21	<8
Sr, Mc, Nt, Tr	2016 September 9	57640.67	57641.19	<8
Sr, Mc, Nt, Tr	2016 September 10	57641.54	57641.83	<8
Mc, Nt, Tr, On	2016 September 23	57654.50	57655.15	<20

[a]The observations are split to report the different flux density values but they correspond to the same run.

phase-referenced data, we did not find any significant peak in the image plane. Upper limits are reported in Table 3. Conservatively, we determined upper limits from the lack of fringe detections at 5σ significance in 2.5 min on the most sensitive baseline, based on the EVN online calculator.[5] This is a more conservative approach than reporting the image rms noise. The latter is typically much lower but could underestimate the true source flux density in case of (1) variability on time-scales shorter than the observation duration or (2) significant coherence losses due to imperfect phase referencing. These results are in agreement with the light curve obtained with the RATAN-600 at lower frequencies; the flux densities are between 10 and 40 mJy at 2.3, 4.6, 8.2 and 11.2 GHz (Trushkin et al. 2017), which indicates a quenched radio state. The hard X-ray emission (*Swift*/BAT light curve) confirms the persistent ultra-soft state of the source during this period (see Fig. 1).

The case of the 2016 September 23 observation (last VLBI trigger) is more complex. SRT could not participate in the session due to technical problems following a storm. The fringe detection threshold therefore became significantly larger, probably around 15–20 mJy. Cyg X-3 was not detected even though the calibrators were correctly observed during the session. A summary of the five VLBI observations is presented in Table 3.

4 DISCUSSION

4.1 X-ray and radio connections in 2016 August/September

Ejection processes are closely linked to accretion in X-ray binaries, but the mechanisms at the origin of the launch of relativistic jets are not well established (Fender, Belloni & Gallo 2004; Markoff, Nowak & Wilms 2005).

The hard X-ray light curve (15–50 keV) extracted from *Swift*/BAT indicated that the flux of Cyg X-3 dramatically dropped starting from 2016 August 15 (MJD 57615) to reach an ultra-soft state (∼0.01 Crab flux) a few days later (see Fig. 1). The hardness ratio and X-ray light curves obtained with MAXI (2–4 keV) and *Swift*/BAT highlight changes of states in Cyg X-3, from the ultra-soft to the soft state during the giant flare (maximum of the peak on MJD 57650), then from the soft to the hard state at the end of the event (MJD 57660). This favours changes in the accretion rate, likely related to variations in the mass-loss from the dense stellar wind associated with the Wolf–Rayet companion star (Kitamoto et al. 1994; Watanabe et al. 1994; Gies et al. 2003).

[5] http://www.evlbi.org/cgi-bin/EVNcalc.pl

The quenching of the jet in the ultra-soft X-ray state could be a direct consequence of high accretion rates, with the inner radius of the disc approaching very close to the compact object (Hjalmarsdotter et al. 2009). Giant flares mark the end of this state and the transition to the soft state (Corbel et al. 2012). In this way, they became predictable events (Koljonen et al. 2010; Trushkin et al. 2016a).

A correlation may be present between the duration of the ultra-soft state and the strength of the subsequent radio flare. The two last giant flares in 2011 March and 2016 September had an extensive radio and X-ray monitoring that covered the full duration of the events. The 2011 March flare followed a very long ultra-soft state of ∼36 d, reached a peak flux density of ∼20 Jy at 15 GHz, doubling the 2016 September flare flux density (∼10 Jy at 18.6 GHz) that occurred after a much shorter ultra-soft state (∼23 d). Even for the multiple flares in 2006, the stronger double radio event in May peaking at ∼14 Jy at 15 GHz is preceded by a longer ultra-soft state (∼41 d) with respect to the July event (∼7 Jy at 11.2 GHz and <20 d ultra-soft state).

4.2 A small flare precursor to the giant flare

While Cyg X-3 was in the ultra-soft state, the hard X-ray flux suddenly increased for the 3 d following 2016 August 29 (∼0.05 Crab flux), before decreasing again on September 1 (see Fig. 1). Fast variations of the flux density were detected at 22 GHz during the first VLBI session triggered on the same day (MJD 57632.7). Fig. 9 shows the presence of two peaks of ∼440 and ∼250 mJy with a duration of 2 h each, while the off-peaks indicate a general diminution of the flux density. Images of the emitting component obtained during the first 4 h of the observation highlighted an increase of the emission size from 0.6 to 0.9 mas (radius), as shown in Figs 7 and 8 at the moment of the first peak at ∼440 mJy during the mini-flare. We measured an expansion of 0.3 mas in radius in 4 h, equivalent to a velocity of 0.07–0.09c, assuming a distance to the source at 7–9 kpc. This velocity appears to be slower than the sound speed in mildly relativistic plasma and could be associated with the presence of a wind rather than a jet. The source was not detected during the VLBI observation performed a few days later, on September 3, 9 and 10 (upper limit of 8 mJy at 22 GHz).

The RATAN-600 light curve confirmed the presence of a mini-flare (Trushkin et al. 2017) that started on August 30 and lasted for ∼4 d before Cyg X-3 came back to the quenched state (∼30 mJy at 11.2 GHz). The peak reached a maximum of ∼600–700 mJy at 8.2–11.2 GHz and ∼300 mJy at 4.6 GHz on September 1 (Trushkin et al. 2017). Our VLBI data obtained on 2016 September 1 correspond to the very beginning of the declining phase of the small flare,

about 10 d before the onset of the rising phase of the giant flare. The short-duration flare occurred close to the core, with an evidence of a very slight extension of the wind or jet. Similar small radio flares have often been observed prior to giant flare events of Cyg X-3 (Waltman et al. 1994, 1995; Newell, Garrett & Spencer 1998; Kim et al. 2013). In particular, a VLBI observation performed in 2007 during a short-live flare (3 h) with a flux density of 1.6 Jy gives similar results. The analysis of the Gaussian fits to the visibility amplitudes with time bin of 10 min have shown an increase of the source size or a structural change during the mini-flare (Kim et al. 2013). In both cases, we note that the emitting size slightly increases from the peak of the mini-flare until the end of the flare. As a consequence, the maximum of the flux density is reached before the small expansion of the wind or jet occurred.

4.3 Spectral index evolution during the giant flare

Single-dish observations of Cyg X-3 show evidence of flux density variations on a time-scale of a few hours. The variations observed in the 7.2–8.5 and 18.6–25.6 GHz light curves do not follow the same trend, in particular at the peak maximum, on 2016 September 19. While the flux density at lower frequencies remains quite stable, fast changes are observed at higher frequencies. The evolution of the spectral index testifies the high variability of the source. The spectral index flattens ($\alpha \sim 0.3$) during the rise of the source flux, while it steepens ($\alpha \sim 0.6$) when the source flux declines at high frequencies. We note that the values of the spectral index are very similar to the ones associated with previous giant flares (Miller-Jones et al. 2004, and references therein) and with low-level flare events (Miller-Jones et al. 2009). However, the spectral steepening over a time-scale of hours is for the first time highlighted. Miller-Jones et al. (2004) studied several hypotheses based on energy-dependent loss mechanisms to explain the steepening on the scale of a few days. Synchrotron, bremsstrahlung, inverse Compton and leakage (diffusive escape) losses have been ruled out because of the too long time-scales. The only mechanism capable of producing such a spectral evolution is related to light traveltime effects in plasmons (van der Laan 1966). Plasmons would evolve from optically thick to optically thin as they move outward from the core and expand. A flat-spectrum core component dominates the flux density initially but fades over time. A steep spectral index would be reached when the plasmons become optically thin.

4.4 Comparison between the small and the giant flares

Cyg X-3 was not detected during the last VLBI observation performed at 22 GHz, 4 d after the peak of the giant flare. Medicina recorded a flux density of 3.1 ± 0.1 Jy at 8.5 GHz the same day, while the RATAN-600 detected a radio emission of ∼2 Jy at 21.7 GHz on 2016 September 22 and ∼0.8 Jy on 2016 September 24 (Trushkin et al. 2017). We can estimate the expected flux density at 22 GHz on September 23, considering that the fading of the flare follows an exponential law $\propto \exp[-(t - t_{\rm m})/2{\rm d}]$, where $t_{\rm m} = 57650.7$ the day of the peak maximum. This results in a flux density estimated at ∼1.4 Jy, much higher than the upper limit we inferred for this observation. The source was therefore strongly resolved out at mas scales.

In this way, our VLBI observations give us a direct comparison between the decay phases of the small/short-duration flare and the giant/longer flare in 2016 September. Multifrequency observations carried out with SRT on September 21 indicated that the spectrum of Cyg X-3 was optically thin 2 d after the peak of the flare. Trushkin et al. (2017) confirm this statement and find a clear transition from optically thick to optically thin spectra right after the flare reached its highest brightness. Similar conclusions were drawn in the case of small flares (Miller-Jones et al. 2009). Optically thick spectra are most likely attributed to synchrotron self-absorption or thermal electrons mixed with relativistic ones, whereas optically thin spectra are probably associated with ejecta in expansion moving outwards from the core (Miller-Jones et al. 2009).

The results we obtained with the single-dish and VLBI observations are consistent with the shock-in-jet scenario supported by Lindfors et al. (2007), Miller-Jones et al. (2009) and Türler (2011). These authors suggest that the differences in shape, amplitude, time-scale and frequency range of the flares are related to the strength of the shocks along the jet. Weaker and faster flares are produced closer to the core (Türler, Courvoisier & Paltani 1999) whereas brighter flares evolve on longer time-scales, peak at lower frequencies, and are the consequence of shocks forming further downstream in the jet. Shocks could provide a mechanism for the continuous replenishment of relativistic particles (Atoyan & Aharonian 1999). However, shocks generally give an index of the power-law energy distribution of relativistic particles $p > 2$ or $\alpha > 0.5$ with $\alpha = (p - 1)/2$. While it may be possible to produce a $p < 2$ in shocks, magnetic reconnection in relativistic plasmas with a relatively high magnetization could also explain the change from $p = 1.6$ to 2.2 or $\alpha = 0.3$ to 0.6 (Guo et al. 2014; Sironi & Spitkovsky 2014; Sironi, Giannios & Petropoulou 2016).

The gamma-ray flares detected just before the mini radio flare with AGILE (Piano et al. 2016) and at the very onset of the giant radio flare with *Fermi*/LAT (Cheung & Loh 2016) are also in agreement with our results and with the conclusions drawn from Corbel et al. (2012) during the 2011 March giant flare. The gamma-ray activity is most likely related to shocks appearing at different distances along the jet. Particle acceleration (thanks to shocks or reconnection) happening closer to the core is consistent with a brighter gamma-ray emission than that observed in shocks produced further downstream where the energy density in seed photon decreases, reducing inverse-Compton emission (Dubus, Cerutti & Henri 2010).

4.5 Comparison with previous giant flares

In the following, we try to infer some constraints on the geometry and structure of the jet associated with the fading giant flare on 2016 September 23, based on a comparison with previous giant flares of Cyg X-3. Since the discovery of the first major radio flares by Gregory & Kronberg (1972), Cyg X-3 has gone through a dozen of giant flare episodes exceeding 10 Jy (Waltman et al. 1995, and reference therein). The last five giant flares occurred in 1997 February (Mioduszewski et al. 2001), 2001 September (Miller-Jones et al. 2004), 2006 May–July (Pal, Ishwara-Chandra & Rao 2009; Koljonen et al. 2013), 2011 March (Corbel et al. 2012) and the last one in 2016 September (Trushkin et al. 2017).

High-resolution images obtained with the VLBA clearly demonstrated the complex jet-like structures during the 1997 and 2001 flares. A one-sided jet was detected in the south direction during the 1997 flare, with a speed $\geq 0.81c$ and a precession period ≥60 d (Mioduszewski et al. 2001). The jet emission extended over 50 mas 2 d after the peak of the flare (10 Jy at 15 GHz), and over 120 mas 2 d later. The corresponding synthesized beams were ∼3–5 mas while the proper motion of the jet was >20 mas d^{-1}. This implies a movement by at least two beams during the ∼12 h of the observations, which did not affect the images. VLBA images obtained at 22 GHz during the peak maximum of the 2001 flare revealed a strong core emission (Miller-Jones et al. 2004). The corresponding

flux density was measured at 7.4 Jy with the VLA. A two-sided jet in an almost north–south orientation then appeared the following day, consisting of several discrete knots. A successive observation was triggered 2 d after the peak maximum and confirmed the expansion of the knot sequence with the fading flux density of ∼5 Jy. The proper motions of individual knots, whose initial diameters are ∼8 mas, were measured for the first time and showed evidence of a 5 d jet precession period with a jet speed ∼0.63c.

The angular scale associated with our VLBI observation on 2016 September 23 was ∼1 mas, depending on the projected baseline in the (u, v)-plane. In particular, we estimate a 5σ sensitivity of 20 mJy beam^{-1}, with a beam of 1.4 mas × 0.8 mas full width at half-maximum. This corresponds to a beam area of 0.88 mas^2. The total flux density of the source estimated from the RATAN-600 light curve is 1.4 Jy. If we assume a symmetric, two-sided ejection, our non-detection therefore implies that each of the two $S = 0.7$ Jy features is distributed over a sky area A such that $S/A \leq 5\sigma$; i.e. $A \geq (700\,\mathrm{mJy})/(20\,\mathrm{mJybeam}^{-1}) \sim 35\,\mathrm{beam} \sim 30\,\mathrm{mas}^2$. For a circular component, we thus determine the size of each region to be $\pi r^2 \geq 30\,\mathrm{mas}^2$, or $r \geq 3$ mas. If we further assume that the separation from the core is about 10 × faster than the blob expansion, that implies a distance from the black hole of ≥30 mas, or 3–4 × 10^{15} cm (67 AU), considering a location at 7–9 kpc. Depending on when we assume the time of ejection, it is straightforward to determine a lower limit to the projected jet knot velocity. For example, assuming a blob formation at the peak radio emission as suggested by the change in the spectral index we observed and the clear transition from optically thick to optically thin jet (Trushkin et al. 2017) at that epoch (on September 19), we would obtain a jet speed >0.3c. This is consistent with the plasmon expansion speed derived from previous giant flares. Instead, a later blob formation (≤1 d from this VLBI observation) would imply a superluminal motion.

4.6 The peculiar case of Cyg X-3

A comparison with well-known microquasars shows us that Cyg X-3 represents a unique and somehow very particular source for different reasons. No other X-ray binaries have shown radio flux densities up to ∼20 Jy during giant flare events. Major flares of 1–10 Jy have been observed in some transient black hole X-ray binaries, such as in SS433, V404 Cyg, GRO J1655−40 and A0620−00, all associated with hard-to-soft X-ray transitions. Based on spectral, velocity and morphological characteristics, two types of radio jets have been identified during outbursts, corresponding to different X-ray states (Fender, Homan & Belloni 2009) and so different accretion regimes. *A steady jet* appearing as a bright core (Dhawan, Mirabel & Rodríguez 2000), with a flat or inverted spectrum indicating optically thick self-absorbed synchrotron emission is associated with the hard state (Fender et al. 2004). *A transient jet*, corresponding to the ejection of optically thin radio plasmons moving away from the core of the system at relativistic speeds (Mirabel & Rodríguez 1994), is instead associated with the transition between two types of intermediate states, which are themselves in between the hard and the soft state (Fender et al. 2004). Transitions from steady to transient jet occurs during outbursts, corresponding to an inversion of the spectrum from inverted to optically thin, as also seen in GRS 1915+105 and LS I +61°303.

In the case of Cyg X-3, giant flares occur at the end of the ultra-soft X-ray state (Watanabe et al. 1994) also defined as hyper-soft state by Koljonen et al. (2010), during the transition to a harder state. The jet is found to be optically thick during the rising phase of the giant flare, corresponding to the soft X-ray state, while the jet becomes optically thin at the peak and declining phase of the flare, which corresponds to soft-to-hard state transition (Miller-Jones et al. 2004; Trushkin et al. 2017). A similar transition from the steady to transient jet is therefore observed, however the association with X-ray states is clearly different from other transient X-ray binaries. The presence of strong stellar wind from the companion star could be at the origin of these differences.

GRO J1655−40 shows interesting similarities with Cyg X-3, in particular the presence of the hyper-soft X-ray state that could be associated with very high and unusual rate of accretion close to or above the Eddington limit (Uttley & Klein-Wolt 2015), and strong radio flares up to 10 Jy. GRO J1655−40 is a black hole low-mass X-ray binary that presents the most powerful (possibly magnetically driven) disc wind among the other microquasars. Hard X-ray flares have been detected during the transition from the soft to the ultra-soft X-ray state, and also in the ultra-soft state. The first flare observed in 2005 during the transition from the soft to the ultra-soft state is coincident with an optically thin radio flare which is relatively weak compared to transitional radio flares observed from GRO J1655−40 in earlier outbursts (Kalemci et al. 2016). However, no giant flare has been observed after the 2005 ultra-soft X-ray state.[6]

5 CONCLUSIONS

Cyg X-3 represents an exceptional target that offers the possibility to better understand the relationship between accretion state and jet launching mechanisms, and to compare the effect of accretion geometry (companion star, orbital parameters) to other sources with more typical behaviour, in particular in the extreme cases of giant flares. These very bright and spectacular radio events are rare, clearly associated with the ultra-soft X-ray state and gamma-ray emission. After 5.5 yr of quiescence, a giant flare occurred in 2016 September. Single-dish observations performed with Medicina and SRT followed the evolution of the peak over 6 d in six frequency ranges. The observed frequencies are complementary with the ones used in the RATAN-600. Moreover, the long exposures provided with the Italian radio telescopes allowed us to infer variation of the radio emission on short time-scale. In particular, we highlighted a decline of the flux density at high radio frequency with a steepening of the spectrum from $\nu^{-0.3}$ to $\nu^{-0.6}$ within ∼5 h at the peak of the flare. It is the first time that such a steepening is observed on the hour scale, which gives support to plasmon evolution from optically thick to optically thin as they move outward from the core and expand.

VLBI observations were triggered at 22 GHz at different phases of the 2016 flare episode. Flux variations were detected within 2 h 10 d before the onset of the giant radio flare. They are associated with the declining phase of a mini and short-lived flare produced close to the core. We measured a slight increase of the source size at the moment of the highest peak of the mini-flare. A VLBI observation performed 4 d after the peak of the giant flare allows us to infer constraints on the size and velocity of the jet. The jet emission was most likely extended over 30 mas with a jet knot velocity >0.3c assuming a blob formation at the peak emission as suggested by the change in the spectral index we observed.

The complementarity between single-dish and VLBI observations is essential in order to better understand ejection mechanisms

[6] www.aoc.nrao.edu/mrupen/XRT/GRJ1655-40/grj1655-40.shtml

during giant flare episodes. The data recorded with the recently commissioned SRT confirm its excellent capabilities operating as single-dish and VLBI antenna. The selection of a few EVN telescopes as a EVN lite is very useful to provide VLBI observations of such rare events. For the next giant flares, it would be interesting to perform multifrequency single-dish observations in parallel to VLBI observations from the peak of the flare in order to better track the plasmon evolution from optically thick to optically thin, and directly see the link between changes in the spectral index and jet morphology on relative short time-scales (a few hours). Moreover, it would be more fitted to consider EVN-lite observations at lower frequency during the decay phase of the flare in order to study the morphology, velocity and evolution of the jet.

ACKNOWLEDGEMENTS

The authors would like to thank S. Trushkin for the useful discussions about Cyg X-3. MP acknowledges financial support from the RAS (CRP-25476). SC acknowledges the financial support from the UnivEarthS Labex program of Sorbonne Paris Cité (ANR-10-LABX-0023 and ANR-11- IDEX-0005-02). EK acknowledges support from TUBITAK Grant 115F488. The Sardinia Radio Telescope is funded by the Department of University and Research (MIUR), the Italian Space Agency (ASI) and the Autonomous Region of Sardinia (RAS), and is operated as a National Facility by the National Institute for Astrophysics (INAF). Based on observations with the Medicina telescope operated by INAF – Istituto di Radioastronomia. This work is based in part on observations carried out using the 32-metre radio telescope operated by Torun Centre for Astronomy of Nicolaus Copernicus University in Toruń (Poland) and supported by the Polish Ministry of Science and Higher Education SpUB grant.

REFERENCES

Atoyan A. M., Aharonian F. A., 1999, MNRAS, 302, 253
Belloni T. M., 2010, in Belloni T., ed., The Jet Paradigm, Lecture Notes in Physics, Vol. 794. Springer-Verlag, Berlin, p. 53
Bolli P. et al., 2015, J. Astron. Instrum., 4, 1550008
Bonnet-Bidaud J. M., Chardin G., 1988, Phys. Rep., 170, 325
Cheung C. C., Loh A., 2016, Astron. Telegram, 9502
Corbel S. et al., 2012, MNRAS, 421, 2947
Deller A. T. et al., 2011, PASP, 123, 275
Dhawan V., Mirabel I. F., Rodríguez L. F., 2000, ApJ, 543, 373
Dubus G., Cerutti B., Henri G., 2010, MNRAS, 404, L55
Egron E., Pellizzoni A., Iacolina M. N., Loru S., Righini S., Trois A., SRT Astrophysical Validation Team, 2016a, Internal Report No. 59, INAF – Osservatorio Astronomico di Cagliari
Egron E. et al., 2016b, Astron. Telegram, 9508
Fender R. P., Hanson M. M., Pooley G. G., 1999, MNRAS, 308, 473
Fender R. P., Belloni T. M., Gallo E., 2004, MNRAS, 355, 1105
Fender R. P., Homan J., Belloni T. M., 2009, MNRAS, 396, 1370
Fermi LAT Collaboration, 2009, Science, 326, 1512
Gallo E., Fender R. P., Pooley G. G., 2003, MNRAS, 344, 60
Giacconi R., Gorenstein P., Gursky H., Waters J. R., 1967, ApJ, 148, L119
Gies D. R. et al., 2003, ApJ, 583, 424
Gregory P. C., Kronberg P. P., 1972, Nature, 239, 440
Greisen E. W., 2003, in Heck A., ed., Astrophysics and Space Science Library, Vol. 285, Information Handling in Astronomy – Historical Vistas. Kluwer, Dordrecht, p. 109
Guo F., Li H., Daughton W., Liu Y.-H., 2014, Phys. Rev. Lett., 113, 155005
Hjalmarsdotter L., Zdziarski A. A., Larsson S., Beckmann V., McCollough M., Hannikainen D. C., Vilhu O., 2008, MNRAS, 384, 278
Hjalmarsdotter L., Zdziarski A. A., Szostek A., Hannikainen D. C., 2009, MNRAS, 392, 251
Kalemci E., Begelman M. C., Maccarone T. J., Dinçer T., Russell T. D., Bailyn C., Tomsick J. A., 2016, MNRAS, 463, 615
Kim J.-S., Kim S.-W., Kurayama T., Honma M., Sasao T., Kim S. J., 2013, ApJ, 772, 41
Kitamoto S., Miyamoto S., Waltman E. B., Fiedler R. L., Johnston K. J., Ghigo F. D., 1994, A&A, 281, L85
Koch-Miramond L., Ábrahám P., Fuchs Y., Bonnet-Bidaud J.-M., Claret A., 2002, A&A, 396, 877
Koljonen K. I. I., Hannikainen D. C., McCollough M. L., Pooley G. G., Trushkin S. A., 2010, MNRAS, 406, 307
Koljonen K. I. I., McCollough M. L., Hannikainen D. C., Droulans R., 2013, MNRAS, 429, 1173
Krimm H. A. et al., 2013, ApJS, 209, 14
Lindfors E. J., Türler M., Hannikainen D. C., Pooley G., Tammi J., Trushkin S. A., Valtaoja E., 2007, A&A, 473, 923
Ling Z., Zhang S. N., Tang S., 2009, ApJ, 695, 1111
Markoff S., Nowak M. A., Wilms J., 2005, ApJ, 635, 1203
Martí J., Paredes J. M., Peracaula M., 2001, A&A, 375, 476
McClintock J. E., Remillard R. A., 2006, in Lewin W., van der Klis M., eds, Black Hole Binaries. Cambridge Univ. Press, Cambridge, p. 157
McCollough M. L. et al., 1999, ApJ, 517, 951
McCollough M. L., Corrales L., Dunham M. M., 2016, ApJ, 830, L36
Miller-Jones J. C. A., Blundell K. M., Rupen M. P., Mioduszewski A. J., Duffy P., Beasley A. J., 2004, ApJ, 600, 368
Miller-Jones J. C. A., Rupen M. P., Türler M., Lindfors E. J., Blundell K. M., Pooley G. G., 2009, MNRAS, 394, 309
Mioduszewski A. J., Rupen M. P., Hjellming R. M., Pooley G. G., Waltman E. B., 2001, ApJ, 553, 766
Mirabel I. F., Rodríguez L. F., 1994, Nature, 371, 46
Mirabel I. F., Rodríguez L. F., 1999, ARA&A, 37, 409
Newell S. J., Garrett M. A., Spencer R. E., 1998, MNRAS, 293, L17
Orlati A., Bartolini M., Buttu M., Fara A., Migoni C., Poppi S., Righini S., 2016, in Chiozzi G., Guzman J. C., eds, Proc. SPIE Conf. Ser. Vol. 9913, Software and Cyberinfrastructure for Astronomy IV. SPIE, Bellingham, p. 991310
Ott M., Witzel A., Quirrenbach A., Krichbaum T. P., Standke K. J., Schalinski C. J., Hummel C. A., 1994, A&A, 284, 331
Pal S., Ishwara-Chandra C. H., Rao A. P., 2009, in Saikia D. J., Green D. A., Gupta Y., Venturi T., eds, ASP Conf. Ser. Vol. 407, The Low-Frequency Radio Universe. Astron. Soc. Pac., San Francisco, p. 277
Parsignault D. R. et al., 1972, Nat. Phys. Sci., 239, 123
Perley R. A., Butler B. J., 2013, ApJS, 204, 19
Piano G. et al., 2016, Astron. Telegram, 9429
Prandoni I. et al., 2017, A&A, preprint (arXiv:1703.09673)
Predehl P., Burwitz V., Paerels F., Trümper J., 2000, A&A, 357, L25
Shrader C. R., Titarchuk L., Shaposhnikov N., 2010, ApJ, 718, 488
Sironi L., Spitkovsky A., 2014, ApJ, 783, L21
Sironi L., Giannios D., Petropoulou M., 2016, MNRAS, 462, 48
Szostek A., Zdziarski A. A., 2004, Proc. of X-Ray Timing 2003: Rossi and Beyond
Szostek A., Zdziarski A. A., 2008, MNRAS, 386, 593
Szostek A., Zdziarski A. A., McCollough M. L., 2008, MNRAS, 388, 1001
Tavani M. et al., 2009, Nature, 462, 620
Trushkin S. A., Nizhelskij N. A., Tsybulev P. G., Zhekanis G. V., 2017, in Balega Yu. Yu., Kudryavtsev D. O., Romanyuk I. I., Yakunin I. A., eds, ASP Conf. Ser. Vol. 510, Stars: From Collapse to Collapse. Astron. Soc. Pac., San Francisco, p. 492
Trushkin S. A., Nizhelskij N. A., Tsybulev P. G., Zhekanis G. V., 2016a, Astron. Telegram, 9416
Trushkin S. A., Nizhelskij N. A., Tsybulev P. G., Zhekanis G. V., 2016b, Astron. Telegram, 9501
Tudose V. et al., 2007, MNRAS, 375, L11
Türler M., 2011, Mem. Soc. Astron. Ital., 82, 104
Türler M., Courvoisier T. J.-L., Paltani S., 1999, A&A, 349, 45
Uttley P., Klein-Wolt M., 2015, MNRAS, 451, 475
van der Laan H., 1966, Nature, 211, 1131
van Kerkwijk M. H., Geballe T. R., King D. L., van der Klis M., van Paradijs J., 1996, A&A, 314, 521

Waltman E. B., Fiedler R. L., Johnston K. J., Ghigo F. D., 1994, AJ, 108, 179
Waltman E. B., Ghigo F. D., Johnston K. J., Foster R. S., Fiedler R. L., Spencer J. H., 1995, AJ, 110, 290
Waltman E. B., Foster R. S., Pooley G. G., Fender R. P., Ghigo F. D., 1996, AJ, 112, 2690
Watanabe H., Kitamoto S., Miyamoto S., Fielder R. L., Waltman E. B., Johnston K. J., Ghigo F. D., 1994, ApJ, 433, 350
Zdziarski A. A., Segreto A., Pooley G. G., 2016, MNRAS, 456, 775

This paper has been typeset from a TEX/LATEX file prepared by the author.